Geology, published online on 22 July 2013 as doi:10.1130/G34483.1

# Silica gel formation during fault slip: Evidence from the rock record

J.D. Kirkpatrick[1*], C.D. Rowe[2], J.C. White[3], and E.E. Brodsky[1]
[1]Earth & Planetary Sciences Department, University of California–Santa Cruz, 1156 High Street, Santa Cruz, California 95064, USA
[2]Department of Earth & Planetary Sciences, McGill University, 3450 University Street, Montréal, Québec H3A 0E8, Canada
[3]Department of Earth Sciences, University of New Brunswick, 2 Bailey Drive, Fredericton, New Brunswick E3B 5A3, Canada

## ABSTRACT

**Dynamic reduction of fault strength is a key process during earthquake rupture. Many mechanisms for causing coseismic weakening have been proposed based on theory and laboratory experiments, including silica gel lubrication. However, few have been observed in nature. Here we report on the first documented occurrence of a natural silica gel coating a fault surface. The Corona Heights fault slickenside in San Francisco, California, is covered by a shiny layer of translucent silica. Microstructures in this layer show flow banding, armored clasts, and extreme comminution compared to adjacent cataclasites. The layer is composed of ~100 nm to 1 µm grains of quartz, hydrous crystalline silica, and amorphous silica, with 10–100 nm inclusions of Fe oxides and ellipsoidal silica colloids. Kinematic indicators and mixing with adjacent cataclasites suggest the shiny layer was fluid during fault slip. The layer therefore represents a relict silica gel that formed during fault motion, and which could have resulted in frictional instability. These observations confirm that the silica gels formed in rock friction experiments do occur in natural faults and therefore that silica gel formation can act as a dynamic weakening mechanism in faults at shallow crustal conditions.**

## INTRODUCTION

Dynamic reduction of fault strength as a function of slip or slip rate is fundamental to earthquake propagation and slip (Rice, 2006). Silica gel lubrication (Goldsby and Tullis, 2002) is one of a variety of mechanisms that have been proposed to cause coseismic weakening based on theoretical and experimental work (e.g. Sibson, 1973; Brodsky and Kanamori, 2001; Di Toro et al., 2006; Rice, 2006; Han et al., 2007; Brantut et al., 2008), but only a handful of these mechanisms are documented in nature (e.g., Di Toro et al., 2006; Rowe et al., 2012). As silica is a major component of crustal rocks, silica gel lubrication is a particularly attractive mechanism, yet field evidence has been elusive.

Experiments on silica-rich rocks (chert and quartzite) show that steady-state friction values decrease with slip rate from ~0.6 at $10^{-6}$ m/s to <0.2 at >$10^{-3}$ m/s, and show time-dependent strengthening (Goldsby and Tullis, 2002; Di Toro et al., 2004; Hayashi and Tsutsumi, 2010; Nakamura et al., 2012). The slip-weakening behavior is explained by the formation of a thixotropic gel on the slip interface, which is frequently invoked as a potentially important process for shallow crustal faults (Di Toro et al., 2004). The presence of gel is supported by observations of silica displaying flow structures (Niemeijer et al., 2012) and X-ray diffraction (XRD) and Raman microspectroscopy analyses demonstrating the formation of amorphous hydrous silica on the slip surface (Hayashi and Tsutsumi, 2010; Nakamura et al., 2012).

However, no clear natural examples of gels formed in situ along natural fault surfaces have been documented, so the significance of silica gel lubrication as a dynamic weakening mechanism remains unknown. Opaline veins that may have formed as silica gels occur in faults associated with hydrothermal systems (Power and Tullis, 1989; Stel and Lankreyer, 1994; Caine et al., 2010) and possible slip-surface gels have been described elsewhere (e.g., Ujiie et al., 2007; Faber et al. 2009), but the distinguishing characteristics, mechanisms for gel formation from a solid rock, and the relationship to fault slip have not been shown.

Here, we present observations of a distinctive silica layer coating a fault slickenside. The Corona Heights fault, in San Francisco, California, is an oblique-dextral fault that cuts chert of the Marin Headlands terrane of the Franciscan Complex, a rock similar to the novaculite used in the gel-producing experiments. Exposed by quarrying around the end of the 19th century, the fault has a mirror-like finish due to the presence of a 1–3-mm-thick layer of vitreous silica. We describe the micro- to nano-scale structure of this layer and evaluate the potential that it represents a natural example of silica gel formation.

## COMPOSITION AND MICROSTRUCTURE OF THE SHINY LAYER

The fault is exposed in a 15-m-high cliff striking ENE-WSW, and can be traced for ~300 m along strike across the Corona Heights Park (Fig. 1A). No offset markers have been observed so the total offset on the fault is unconstrained. The dark red radiolarian chert host rock has been metamorphosed to prehnite-pumpellyite facies conditions (Meneghini and Moore, 2007), indicating peak temperatures >200 °C. Radiolarian tests are recrystallized to microcrystalline quartz, and XRD spectra confirm that only α-quartz and

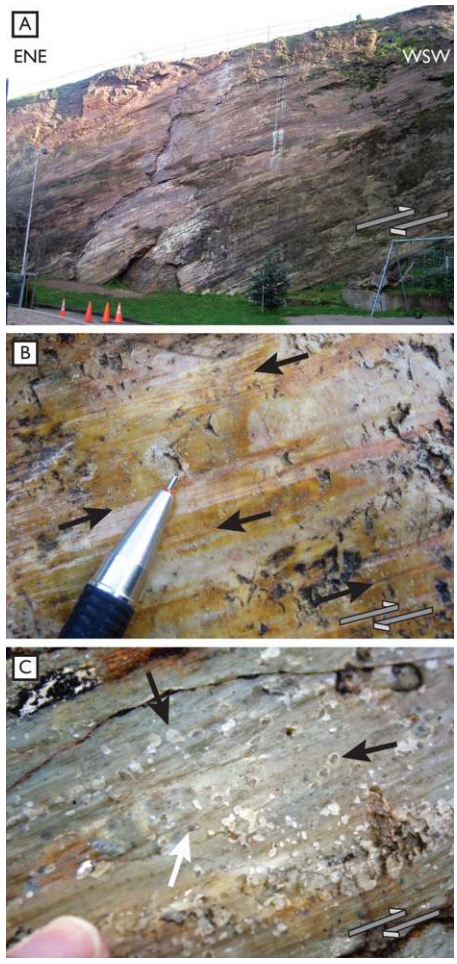


**Figure 1. A: Photograph of slickenside exposed in Corona Heights Park, San Francisco, California, which is 10 km from trace of San Andreas fault (37.7654°N, 122.4371°W). Corrugations on the surface rake ~30° to northeast (down to the left in this field of view). Large fractures cutting the face coincide with branch lines between anastomosing fault surfaces. B: Grooves contained within shiny layer (arrows). The shiny silica layer covering the slickenside is translucent; colors are from cataclasite behind the layer. C: Circular fractures within the shiny layer are commonly centered on chert clasts (black arrows). Clasts (white arrow) and fractures are sometimes arranged in linear clusters aligned parallel to grooves.**

*Current address: Department of Geosciences, Colorado State University, 1482 Campus Delivery, Fort Collins, Colorado 80523, USA.

Fe oxides and hydroxides are detectable in the chert (see the GSA Data Repository[1]).

The slickenside surface is shiny due to the presence of a 0.5–3.0-mm-thick layer of translucent, vitreous silica. The shiny layer overlies red or white cataclasites, the color varying with the iron content and oxidation state of chert clasts. Fine grooves within the shiny layer form elongate troughs up to 5–10 cm long, ~1 mm wide, and <1 mm deep, oriented parallel to corrugations with centimeter-scale amplitudes (Fig. 1B). Together, these features define the short-wavelength roughness of the surface, which is self-affine (Candela et al., 2011). Circular cracks within the shiny layer are visible on the slickenside face. These cracks are often centered on small (<1 mm) fragments and locally form elongate clusters strung out parallel to the groove direction (Fig. 1C).

The shiny layer contains angular to rounded chert clasts in a matrix of mixed aphanitic and microcrystalline silica (Figs. 1C and 2). Flow banding in the matrix, defined by variations in iron oxide content and grain size of the silica, wraps around clasts. A set of bands ~10–50 µm wide, defined by preferred crystallographic orientation in the silica (*c*-axis parallel to the band margins in a plane perpendicular to the fault surface), forms angles of ~80°–90° to the edge of the layer in the X-Z plane (Fig. 2; similar to those reported by Power and Tullis [1989] and Caine et al. [2010]). Subsidiary shears at 20°–25° to the slip surface cross cut and offset all of the features in the shiny layer. Optically visible clasts ranging from a few tens of micrometers to 1 mm make up ~10% of the layer. Clasts consist of chert and more frequently fragments of cataclasite or reddish brown aphanitic silica. Some larger clasts have a cortex of similar reddish brown aphanitic silica (Fig. 2C).

The matrix of the layer consists of roughly hexagonal aggregates from <1 to 5 µm in size separated by micrometer-scale, angular pores (Fig. 2D). The aggregates are composed primarily of <100–300 nm grains of silica exhibiting various degrees of crystallinity (Fig. 3), as is evident from transmission electron microscope (TEM) diffraction patterns that show wider deviations in crystal structure (d-spacings) than justified by instrumental parameters. Silica phases recognized within the shiny layer include well-structured quartz, crystalline silica (locally hydrous, based on vulnerability to electron beam damage and TEM diffraction patterns) exhibiting quartz-like properties but with considerable inconsistency in crystal parameters, and clearly amorphous silica.

[1]GSA Data Repository item 2013283, Marin Headlands terrane chert photomicrographs and XRD spectra, is available online at www.geosociety.org/pubs/ft2013.htm, or on request from editing@geosociety.org or Documents Secretary, GSA, P.O. Box 9140, Boulder, CO 80301, USA.

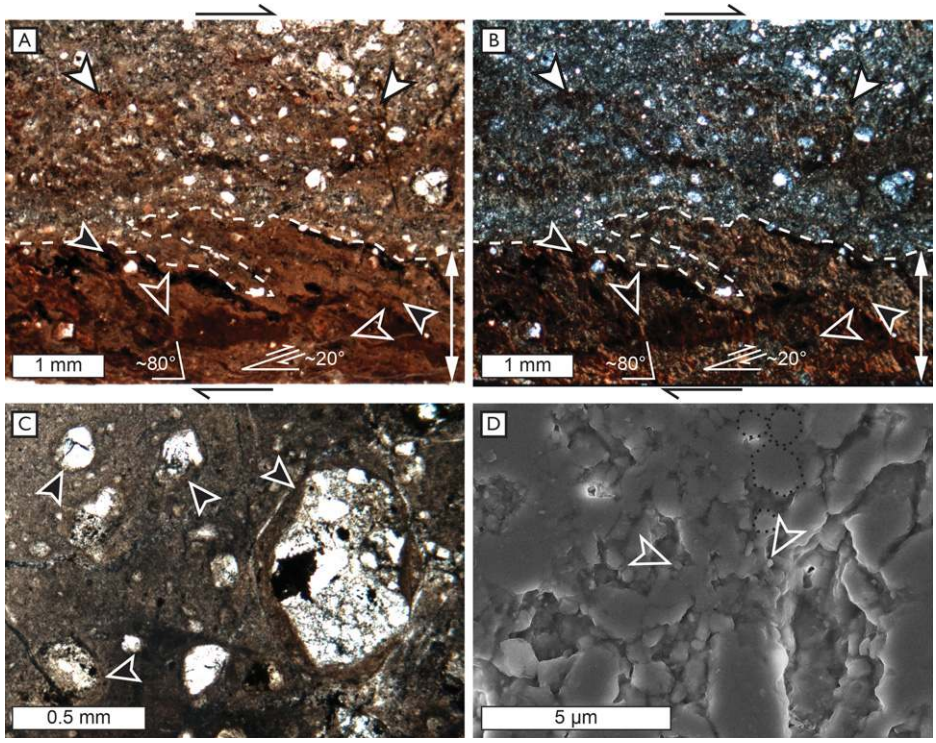


**Figure 2. A: Plane light photomicrograph of shiny layer (shown by vertical white arrow) and adjacent cataclasite. Fault surface is at base of image, parallel to lower edge. Flow banding, defined by more opaque or reddish layers, wraps around clasts (black arrows). The sharp irregular boundary between the layer and cataclasites is shown by dashed line. Note banded appearance of shiny layer (open arrowheads, angle to fault plane shown). The same matrix material is distributed throughout adjacent cataclasites in wispy bands (white arrowheads). Elsewhere, cataclasites are composed of fragmented chert and silica at all scales of observation. B: Same image as in A, in cross-polarized light. C: Grains of broken cemented cataclasite in shiny layer with cortexes of silica and Fe oxides (arrows). D. Field emission scanning electron microscopy image of face of polished section of silica in shiny layer showing roughly hexagonal grains (e.g., black dashed lines) with abundant anhedral, sub-micrometer grains visible in pore spaces (arrowheads).**

Amorphous silica exists as blebs surrounded by anhedral crystalline silica grains (Fig. 3A). Anhedral silica grains exhibit coherent electron scattering typical of long-range order and contain elliptical to hexagonal cells of slightly different crystallographic orientation (Fig. 3B). Cell boundaries are defined by variations in scattering contrast with no extended defects imaged. Induced ionization damage preferentially affects the cell boundaries, consistent with them comprising more hydrous material. Ellipsoidal crystalline silica and euhedral quartz grains 10–100 nm long are common inclusions within both cells and larger crystalline silica grains. Intracrystalline dislocations are rare in all phases, and form sessile loops characteristic of primary growth defects rather than deformation-induced dislocations. Elongate, nanometer-scale pores lie along grain boundaries between the ~100–300 nm grains. Elliptical grains of Fe oxides (and possibly hydroxides) ≤10 nm long are common. They are distributed throughout the layer and are occasionally arranged with long axes aligned in elliptical rings (Fig. 3C).

The fine grain size, flow banding, and Fe oxide content differentiate the vitreous silica layer from adjacent cataclasites. The boundary between the shiny layer and adjacent cataclasites is interfingered and embayed, indicative of local mixing. In places the cataclasites are partially cemented with fine-grained quartz that resembles the shiny layer, but most of the cataclasites are clast rich with a granular matrix (Figs. 2A and 2B).

## RELICT GEL

The shiny slickenside layer on the Corona Heights fault is composed of amorphous silica, hydrous crystalline silica grains locally containing cellular structures, quartz, and nanoparticles of Fe oxide. The textural relationships between these grains suggest progressive transformation of primary amorphous patches to more-ordered silica phases that have grown at the expense of the amorphous hydrous silica (Fig. 3).

Two features record the presence of colloidal silica particles within the layer when it formed (Fig. 3). The cells in the hydrous silica grains reflect nucleation of crystalline material onto

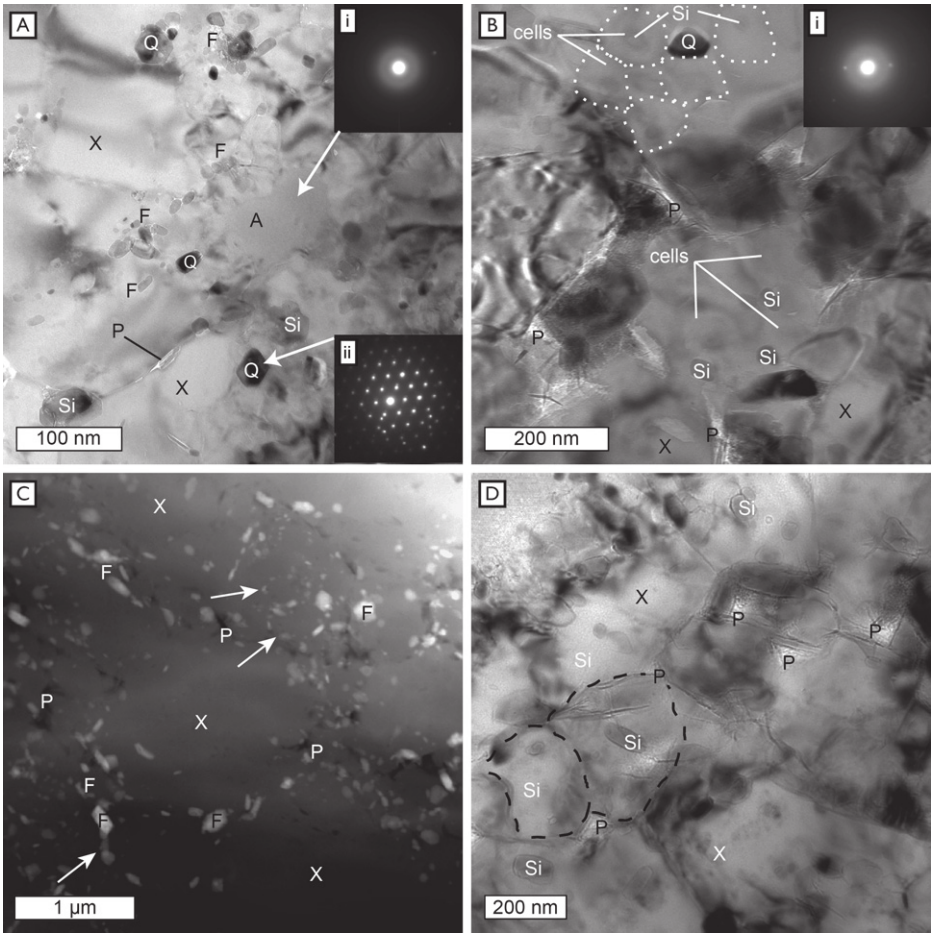


**Figure 3. Transmission electron microscopy (TEM) images of shiny layer. Foils were prepared parallel to fault slip surface within shiny layer. A—amorphous hydrous silica; X—hydrous crystalline silica; P—pores; Si—ellipsoidal silica inclusion (unknown phase); Q—quartz crystal; F—iron oxide grain. A: Bright-field TEM image showing amorphous hydrous silica surrounded by 100–200 nm crystalline hydrous silica grains (X) with inclusions (Si and F). Inset: Diffraction patterns from gray amorphous area (i) and quartz crystal (ii) (B = [0001]). B: Bright-field TEM image showing hydrous crystalline silica crystals (X) with subtle cellular structure within grains (examples are outlined; compare to center of image). Silica particles acting as nuclei are indicated (Si). Inset: Diffraction pattern exhibiting significant inelastic scattering with a broad intensity ring localized at g = (101) typical of transitions from incoherent scattering in amorphous material to wholly crystalline quartz, as observed in A. C: High-angle, dark-field scanning TEM image showing iron oxide or hydroxide grains (F; light gray to white) and elongate pores (P; black) concentrated along and around grain boundaries of hydrous crystalline silica grains (X; dark gray). Arrows indicate ellipsoidal arrangement of oxide inclusions, indicating inclusion of oxide-lined silica within larger silica grain. D: Well-developed cellular structure (similar to B; black dashed lines) with independent grain boundaries, separated by pores (P) at triple junctions and along grain boundaries.**

colloidal particles within the initially amorphous material. The ring arrays of Fe oxide grains show the adherence of secondary phases to the outside of primary colloids. Subsequent transformation produced more fully crystalline material with straight grain boundaries, hexagonal grain shapes, and grain-boundary pores. The absence of deformation-induced dislocations in all phases in the shiny layer indicates that the crystallinity of most silica postdates fault slip, consistent with growth from an amorphous, syndeformational precursor. This also suggests the bands of preferred crystallographic orientation postdate slip. As hydrous silica is less dense than quartz, we hypothesize that the circular fractures centered on chert clasts were formed by shrinkage of the gel layer during solidification and dewatering.

Together, these observations show that the shiny layer solidified from silica-supersaturated fluid containing colloidal silica particles with impurities (Fe oxides) segregated into discrete grains (cf. Herrington and Wilkinson, 1993). These characteristics define a sol or gel, and we therefore suggest the translucent layer is a relict silica gel (sensu Goldsby and Tullis, 2002).

Three lines of evidence demonstrate the silica gel was generated during fault slip rather than being sourced from a hydrothermal fluid, as is inferred elsewhere (Power and Tullis, 1989). First, the deformation structures in the shiny layer (slickenlines and linear arrays of clasts visible in exposure, and subsidiary shears and flow banding in thin section) are kinematically consistent with the larger-scale slip indicators on the fault. Second, the armored clasts and mixing with the cataclasite suggest the silica layer was fluid simultaneous with cataclastic flow in the cataclasite layer. Third, the mineralogy of the layer (silica + Fe oxides) is identical to the wall rock, so there is no evidence for the introduction of a foreign fluid.

Rock friction experiments demonstrate that silica-rich rocks form gels at moderate to high slip rates by frictional wear in only ambient air humidity (Hayashi and Tsutsumi, 2010; Nakamura et al., 2012). Silica must amorphize and hydrate during slip to form a gel. Di Toro et al. (2011) suggested that cataclasis during the rock friction experiments facilitates hydrolization and amorphization by generating fresh, reactive quartz surfaces to generate silica gel. Silica (α-quartz) amorphization is also observed under static pressures (25–35 GPa; Hemley et al., 1988), and at a variety of applied stresses, bulk displacement rates, and temperatures (Yund et al., 1990; White et al. 2009; Pec et al., 2012). The hydrated amorphous silica and relict colloids documented here most closely resemble the products of the rock friction experiments, suggesting a cataclastic origin. Because the entire Corona Heights fault surface is covered by the shiny layer, the rate of production of cataclastic particles must have been high compared to the rate of aggregation, indicating the material formed at elevated slip rates.

Amorphous and intermediate crystalline forms of silica are rapidly recrystallized at low temperatures (<100 °C) experimentally (Oehler, 1976) and in sedimentary systems (Williams and Crerar, 1985). Apatite fission-track data (Dumitru, 1989) indicate the country rocks cooled below ~100 °C at ca. 43 Ma, constraining the maximum likely age of the relict gel. Neogene and younger geothermal gradients in northern California are 25–30 °C/km (Lachenbruch and Sass, 1980), so activity on the Corona Heights fault probably occurred at ≤4 km depth.

If the relict gel had a similar rheology to the experimentally derived material, it may be evidence for earthquake slip weakening and a paleo-earthquake on the Corona Heights fault. The onset of weakening occurs at velocities greater than ~1 mm/s (e.g., Di Toro et al., 2004), which corresponds to slow earthquake or seismic slip rates (Rowe et al., 2011). However, there is no direct observation from the experiments that constrains the specific work, slip magnitude, or strain rate at which gel forms. As we have no independent constraint on the slip rate on the Corona Heights

fault, the gel could have formed during creep without resulting in dramatic weakening. Further experimental and microstructural work is required to establish if the textures we describe formed during a paleo-earthquake. We conclude that the presence of a relict silica gel over the surface of the Corona Heights fault shows that silica gel does form and can dynamically weaken natural faults during slip.

**ACKNOWLEDGMENTS**

Field emission scanning electron microscopy (SEM) images were obtained at NASA–Ames through NASA grant NNX09AQ44A to the University of California–Santa Cruz (UCSC) for the instruments in the UCSC Materials Analysis for Collaborative Science (MACS) Facility within the Advanced Studies Laboratories. Thanks to Joey Varelas at the UCSC MACS Facility for help with SEM imaging. Louise Weaver and the staff of the Microscopy and Microanalysis Facility at the University of New Brunswick provided support for transmission electron microscopy. Matej Pec, Virginia Toy, and an anonymous reviewer provided constructive reviews that greatly improved this paper. This work was supported by National Science Foundation grant EAR0948740 and Natural Sciences and Engineering Research Council of Canada Discovery grants to C. Rowe and J.C. White.

**REFERENCES CITED**

Brantut, N., Schubnel, A., Rouzaud, J.-N., Brunet, F., and Shimamoto, T., 2008, High-velocity frictional properties of a clay-bearing fault gouge and implications for earthquake mechanics: Journal of Geophysical Research, v. 113, B10401, doi:10.1029/2007JB005551.

Brodsky, E.E., and Kanamori, H., 2001, Elastohydrodynamic lubrication of faults: Journal of Geophysical Research, v. 106, p. 16,357–16,374, doi:10.1029/2001JB000430.

Caine, J.S., Bruhn, R.L., and Forster, C.B., 2010, Internal structure, fault rocks, and inferences regarding deformation, fluid flow, and mineralization in the seismogenic Stillwater normal fault, Dixie Valley, Nevada: Journal of Structural Geology, v. 32, p. 1576–1589, doi:10.1016/j.jsg.2010.03.004.

Candela, T., Renard, F., Bouchon, M., Schmittbuhl, J., and Brodsky, E.E., 2011, Fault slip distribution and fault roughness: Geophysical Journal International, v. 187, p. 959–968, doi:10.1111/j.1365-246X.2011.05189.x.

Di Toro, G., Goldsby, D.L., and Tullis, T.E., 2004, Friction falls towards zero in quartz rock as slip velocity approaches seismic rates: Nature, v. 427, p. 436–439, doi:10.1038/nature02249.

Di Toro, G., Hirose, T., Nielsen, S., Pennacchioni, G., and Shimamoto, T., 2006, Natural and experimental evidence of melt lubrication of faults during earthquakes: Science, v. 311, p. 647–649, doi:10.1126/science.1121012.

Di Toro, G., Han, R., Hirose, T., De Paola, N., Nielsen, S., Mizoguchi, K., Ferri, F., Cocco, M., and Shimamoto, T., 2011, Fault lubrication during earthquakes: Nature, v. 471, p. 494–498, doi:10.1038/nature09838.

Dumitru, T.A., 1989, Constraints on uplift in the Franciscan subduction complex from apatite fission track analysis: Tectonics, v. 8, p. 197–220, doi:10.1029/TC008i002p00197.

Faber, C., Rowe, C.D., Miller, J.A., Backeberg, N., and Sylvester, F., 2009, Possible silica gel in the Olive Fault, Naukluft Nappe Complex, Namibia: A geologic record of dynamic weakening in faults during continental orogenesis: Eos (Transactions, American Geophysical Union), v. 90, no. 52, Fall Meeting Supplement, abstract T53C-1606.

Goldsby, D.L., and Tullis, T.E., 2002, Low frictional strength of quartz rocks at subseismic slip rates: Geophysical Research Letters, v. 29, 1844, doi:10.1029/2002GL015240.

Han, R., Shimamoto, T., Hirose, T., Ree, J.-H., and Ando, J.-i., 2007, Ultralow friction of carbonate faults caused by thermal decomposition: Science, v. 316, p. 878–881, doi:10.1126/science.1139763.

Hayashi, N., and Tsutsumi, A., 2010, Deformation textures and mechanical behavior of a hydrated amorphous silica formed along an experimentally produced fault in chert: Geophysical Research Letters, v. 37, L12305, doi:10.1029/2010GL042943.

Hemley, R.J., Jephcoat, A.P., Mao, H.K., Ming, L.C., and Manghnani, M.H., 1988, Pressure-induced amorphization of crystalline silica: Nature, v. 334, p. 52–54, doi:10.1038/334052a0.

Herrington, R.J., and Wilkinson, J.J., 1993, Colloidal gold and silica in mesothermal vein systems: Geology, v. 21, p. 539–542, doi:10.1130/0091-7613(1993)021<0539:CGASIM>2.3.CO;2.

Lachenbruch, A.H., and Sass, J.H., 1980, Heat flow and energetics of the San Andreas fault zone: Journal of Geophysical Research, v. 85, p. 6185–6223, doi:10.1029/JB085iB11p06185.

Meneghini, F., and Moore, J.C., 2007, Deformation and hydrofracture in a subduction thrust at seismogenic depths: The Rodeo Cove thrust zone, Marin Headlands, California: Geological Society of America Bulletin, v. 119, p. 174–183, doi:10.1130/B25807.1.

Nakamura, Y., Muto, J., Nagahama, H., Shimizu, I., Miura, T., and Arakawa, I., 2012, Amorphization of quartz by friction: Implication to silica-gel lubrication of fault surfaces: Geophysical Research Letters, v. 39, L21303, doi:10.1029/2012GL053228.

Niemeijer, A., Di Toro, G., Griffith, W.A., Bistacchi, A., Smith, S.A., and Nielsen, S., 2012, Inferring earthquake physics and chemistry using an integrated field and laboratory approach: Journal of Structural Geology, v. 39, p. 2–36, doi:10.1016/j.jsg.2012.02.018.

Oehler, J.H., 1976, Hydrothermal crystallization of silica gel: Geological Society of America Bulletin, v. 87, p. 1143–1152, doi:10.1130/0016-7606(1976)87<1143:HCOSG>2.0.CO;2.

Pec, M., Stünitz, H., Heilbronner, R., Drury, M., and de Capitani, C., 2012, Origin of pseudotachylytes in slow creep experiments: Earth and Planetary Science Letters, v. 355–356, p. 299–310, doi:10.1016/j.epsl.2012.09.004.

Power, W.L., and Tullis, T.E., 1989, The relationship between slickenside surfaces in fine-grained quartz and the seismic cycle: Journal of Structural Geology, v. 11, p. 879–893, doi:10.1016/0191-8141(89)90105-3.

Rice, J.R., 2006, Heating and weakening of faults during earthquake slip: Journal of Geophysical Research, v. 111, B05311, doi:10.1029/2005JB004006.

Rowe, C.D., Meneghini, F., and Moore, J.C., 2011, Textural record of the seismic cycle: Strain rate variation in an ancient subduction thrust, *in* Fagereng, A., et al., eds., Geology of the Earthquake Source: A Volume in Honour of Rick Sibson: Geological Society of London Special Publication 359, p. 77–95.

Rowe, C.D., Fagereng, Å., Miller, J., and Mapani, B., 2012, Signature of coseismic decarbonation in dolomitic fault rocks of the Naukluft Thrust, Namibia: Earth and Planetary Science Letters, v. 333–334, p. 200–210, doi:10.1016/j.epsl.2012.04.030.

Sibson, R.H., 1973, Interactions between temperature and pore-fluid pressure during earthquake faulting and a mechanism for partial or total stress relief: Nature, v. 243, p. 66–68.

Stel, H., and Lankreyer, A.C., 1994, Flow and deformation of viscous, silica-oversaturated dispersions in low-grade faults: Journal of Structural Geology, v. 16, p. 303–313, doi:10.1016/0191-8141(94)90036-1.

Ujiie, K., Yamaguchi, A., Kimura, G., and Toh, S., 2007, Fluidization of granular material in a subduction thrust at seismogenic depths: Earth and Planetary Science Letters, v. 259, p. 307–318, doi:10.1016/j.epsl.2007.04.049.

White, J.C., Hadizadeh, J., Tullis, T.E., and Goldsby, D.L., 2009, Mechanical amorphization during experimental shearing of synthetic granite gouge: European Geosciences Union Geophysical Research Abstracts, v. 11, p. EGU2009-8996.

Williams, L.A., and Crerar, D.A., 1985, Silica diagenesis; II. General mechanisms: Journal of Sedimentary Research, v. 55, p. 312–321.

Yund, R. A., Blanpied, M. L., Tullis, T. E., and Weeks, J. D., 1990, Amorphous material in high strain experimental fault gouges: Journal of Geophysical Research, v. 95, p. 15,589–15,602, doi:10.1029/JB095iB10p15589.

Manuscript received 12 February 2013
Revised manuscript received 10 May 2013
Manuscript accepted 14 May 2013

Printed in USA

Geology

# Silica gel formation during fault slip: Evidence from the rock record

J.D. Kirkpatrick, C.D. Rowe, J.C. White and E.E. Brodsky

*Geology* published online 22 July 2013;
doi: 10.1130/G34483.1



**Notes**